

Towards Accurate Binarization of Diffusion Model

Xingyu Zheng^{*1}, Haotong Qin^{*2}, Xudong Ma¹, Mingyuan Zhang³, Haojie Hao¹,
 Jiakai Wang⁴, Zixiang Zhao⁵, Jinyang Guo¹, Xianglong Liu^{✉1}
¹Beihang University ²ETH Zürich ³Nanyang Technological University
⁴Zhongguancun Laboratory ⁵Xi'an Jiaotong University

Abstract

With the advancement of diffusion models (DMs) and the substantially increased computational requirements, quantization emerges as a practical solution to obtain compact and efficient low-bit DMs. However, the highly discrete representation leads to severe accuracy degradation, hindering the quantization of diffusion models to ultra-low bit-widths. This paper proposes a novel quantization-aware training approach for DMs, namely **BinaryDM**. The proposed method pushes DMs' weights toward accurate and efficient binarization, considering the representation and computation properties. From the representation perspective, we present a *Learnable Multi-basis Binarizer* (LMB) to recover the representations generated by the binarized DM. The LMB enhances detailed information through the flexible combination of dual binary bases while applying to parameter-sparse locations of DM architectures to achieve minor burdens. From the optimization perspective, a *Low-rank Representation Mimicking* (LRM) is applied to assist the optimization of binarized DMs. The LRM mimics the representations of full-precision DMs in low-rank space, alleviating the direction ambiguity of the optimization process caused by fine-grained alignment. Moreover, a quick progressive warm-up is applied to BinaryDM, avoiding convergence difficulties by layerwisely progressive quantization at the beginning of training. Comprehensive experiments demonstrate that BinaryDM achieves significant accuracy and efficiency gains compared to SOTA quantization methods of DMs under ultra-low bit-widths. With 1.1-bit weight and 4-bit activation (W1.1A4), BinaryDM achieves as low as 7.11 FID and saves the performance from collapse (baseline FID 39.69). As the first binarization method for diffusion models, W1.1A4 BinaryDM achieves impressive $9.3\times$ OPs and $24.8\times$ model size savings, showcasing its substantial potential for edge deployment.

1 Introduction

Diffusion models (DMs) [13, 39] have shown excellent capabilities in generation tasks in various fields, such as image [13, 39, 40], vision [24, 12], and speech [26, 30, 15]. With significant generation quality and diversity advantages, DMs have become one of the most popular generative model paradigms. DMs generate data through the iterative noise estimates, while up to 1000 iterative steps slow the inference process and rely on expensive hardware resources. Although some proposed methods can effectively reduce the number of iterations to dozens of times [38, 36, 28, 1], the complex neural network of DMs also results in a large number of floating point calculations and memory usage in each step, which hinders the efficient

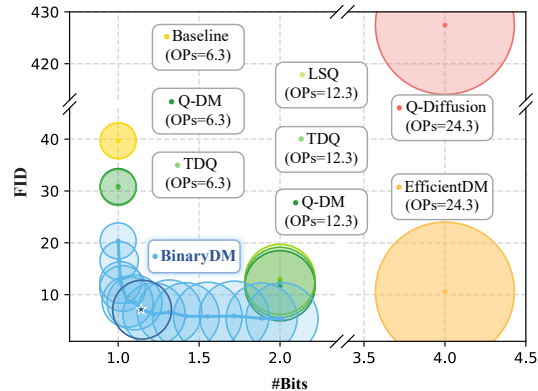


Figure 1: The results under 4-bit activation quantization on LSUN-Bedrooms. BinaryDM enjoys an impressive optimal accuracy-efficiency trade-off.

deployment and inference of DMs on edge. Therefore, the compression of DMs has been widely studied as a practical technology to accelerate the iterative process and reduce the inference cost, including quantization [19, 37], distillation [35, 23, 25], pruning [7], *etc.*

Among them, low-bit quantization emerges as a practical approach to compress deep learning models by reducing the bit-width of parameters [47, 8], and also has satisfactory generality to various network architectures. Thus, with quantization, diffusion models can enjoy the compression and acceleration brought by fixed-point parameters and computation in inference [19, 18, 10, 37]. The 1-bit quantization, namely binarization, allows the binarized model to enjoy compact 1-bit parameters and efficient computation [22, 45, 44]. As the most aggressive bit-width, weight binarization can lead to up to $32\times$ model size reduction and replace expensive floating-point multiplications with addition constructions during inference, thus saving resources and power consumption significantly [33].

However, binarized DMs suffer significant performance degradation compared to their full-precision counterparts. The performance decline primarily arises from two aspects: **First**, weight binarization severely restricts the feature extraction capability of DM, causing significant damage to information in critical representations of generative models. Though several weight binarization methods strive to mitigate binarization errors and enrich representations by floating-point scaling factors [33, 22, 32], the number of candidate values for each weight still drops from 2^{32} to 2^1 . With the homogenized filters, binarization thus makes it hard for the DM to extract patterns in the original input, hindering the construction of output representations with accurate details. **Second**, introducing discrete binarization functions in DM poses a significant hurdle to stable convergence. Existing quantization-aware training methods for DM usually employ direct output-based supervision [19, 10]. However, incorporating binarization introduces errors in parameters and gradients, leading to disruptions in the optimization direction [4, 9]. The crux of the issue lies in the fact that the fine-grained details embedded in the synthetic image or latent code for supervision contribute to the overall optimization process. Unfortunately, the disruptive influence of binarization becomes pronounced in this context, rendering the convergence of DM vulnerable to disturbances and, in some cases, seemingly unattainable.

In this paper, we propose **BinaryDM** to push the weights of diffusion models toward binarization. The proposed method pushes DMs’ weights toward accurate and efficient binarization, considering the representation and computation properties. BinaryDM applies quantization-aware training to binarize DMs accurately for efficient inference, which takes the representation and computation properties of DMs into account and is composed of two novel techniques: *From the representation perspective*, we present a Learnable Multi-basis Binarizer (LMB) to recover the representations generated by the binarized DM. LMB applies dual sets of binary bases with learnable scalars to significantly enhance the feature extraction capability of weights while only applying to parameter-sparse locations of DM architectures selectively to achieve minor burdens. *From the optimization perspective*, a Low-rank Representation Mimicking (LRM) is incorporated to enhance the binarization-aware optimization of DMs. LRM projects binarized and full-precision representations to low-rank, enabling the optimization of binarized DM to focus on the principal direction and mitigate direction ambiguity caused by the representation complexity of generation. Moreover, at the beginning of training, we apply a quick progressive warm-up strategy for BinaryDM, which can accelerate the convergence by layerwisely progressive binarization of DMs.

Comprehensive experiments show that our proposed BinaryDM has significant accuracy and efficiency gains compared to DMs binarized by existing SOTA binarization and low-bit quantization methods. Our BinaryDM can consistently outperform the baseline on DDIM and LDM with 1.1-bit weight, especially with ultra-low bit-width activation. For example, on CIFAR-10 32×32 DDIM, the precision metric of BinaryDM even exceeds the baseline by 49.04% (baseline 2.18% vs. BinaryDM 51.22%) with 1.1-bit weight and 4-bit activation (W1.1A4), saving the binarized DM from collapse. BinaryDM even outperforms the higher bit-width SOTA quantization methods of DM. For LDM-8 on LSUN-Churches 256×256 , W1.1A4 BinaryDM exceeds W4A4 EfficientDM in the FID metric by 4.63. As the first binarization method for DMs, BinaryDM yields impressive $9.3\times$ and $24.8\times$ savings on OPs and model size, demonstrating the vast advantages and potential for deploying the DM on edge.

2 Related Work

Diffusion models (DMs) demonstrate outstanding performance across a diverse range of tasks [13, 39, 40, 29, 26, 30, 15]. However, their slow generation process presents a significant challenge to

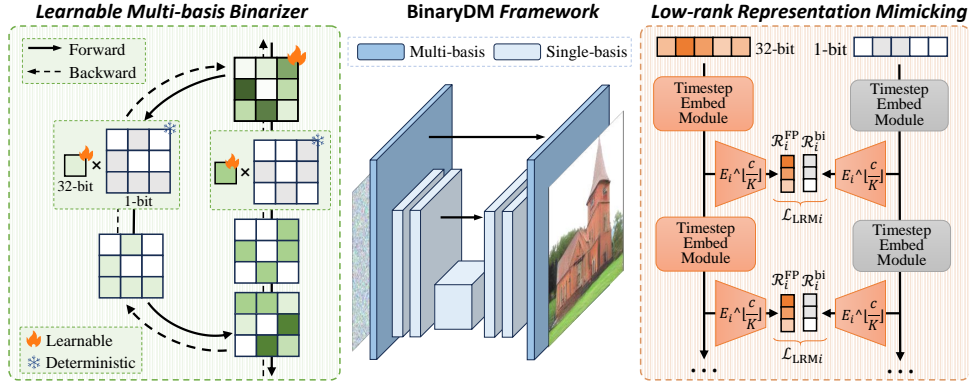


Figure 2: Overview of BinaryDM, consisting of Learnable Multi-basis Binarizer to enhance information representation and Low-rank Representation Mimicking to improve optimization direction.

widespread implementation. Substantial research has focused on reducing the number of time steps to expedite the generation process [42, 3, 39, 40]. Despite the reduction in time steps, denoising models still demand expensive computation and memory for each step.

Quantization and binarization are explored widely as popular compression techniques [27, 20, 43, 21]. These methods involve quantizing the full-precision parameters to lower bit-width (*e.g.*, 1-8 bit). By converting floating-point weights and activations into quantized values, the model size of the neural network can be significantly reduced. This size reduction not only decreases computational complexity but also substantially improves inference speed, memory usage, and energy consumption savings [37, 18]. One notable technique, quantization-aware training [8, 31, 47], involves compressing diffusion models within a training/fine-tuning pipeline to update parameters [19, 10]. Despite these advancements, achieving 1-bit quantization for the weights of DMs remains a formidable challenge. This underscores the need for further research to unlock the potential benefits of 1-bit binarization in DMs. Appendix A presents more details about related works.

3 BinaryDM

3.1 Preliminaries

In the forward process of diffusion models, Gaussian noise is added to data $\mathbf{x}_0 \sim q(\mathbf{x})$ in T times via a schedule β_t controlling noise strength, the process can be expressed as

$$q(\mathbf{x}_t | \mathbf{x}_{t-1}) = \mathcal{N}(\mathbf{x}_t; \sqrt{1 - \beta_t} \mathbf{x}_{t-1}, \beta_t \mathbf{I}), \quad (1)$$

where $\mathbf{x}_t \in \{\mathbf{x}_1, \dots, \mathbf{x}_T\}$ denote the noisy samples at t -th step. The reverse process aims to generate samples by removing noise, approximating the unavailable conditional distribution $q(\mathbf{x}_{t-1} | \mathbf{x}_t)$ with learned distributions $p_\theta(\mathbf{x}_{t-1} | \mathbf{x}_t)$, which can be expressed as

$$p_\theta(\mathbf{x}_{t-1} | \mathbf{x}_t) = \mathcal{N}(\mathbf{x}_{t-1}; \tilde{\boldsymbol{\mu}}_\theta(\mathbf{x}_t, t), \tilde{\boldsymbol{\beta}}_t \mathbf{I}). \quad (2)$$

The mean $\tilde{\boldsymbol{\mu}}_\theta(\mathbf{x}_t, t)$ and variance $\tilde{\boldsymbol{\beta}}_t$ could be derived using the reparameterization tricks in [13]:

$$\tilde{\boldsymbol{\mu}}_\theta(\mathbf{x}_t, t) = \frac{1}{\sqrt{\alpha_t}} \left(\mathbf{x}_t - \frac{1 - \alpha_t}{\sqrt{1 - \bar{\alpha}_t}} \boldsymbol{\epsilon}_\theta(\mathbf{x}_t, t) \right), \quad \tilde{\boldsymbol{\beta}}_t = \frac{1 - \bar{\alpha}_{t-1}}{1 - \bar{\alpha}_t} \cdot \beta_t, \quad (3)$$

where $\alpha_t = 1 - \beta_t$, $\bar{\alpha}_t = \prod_{i=1}^t \alpha_i$, and $\boldsymbol{\epsilon}_\theta$ denotes a function approximation with the learnable parameter θ , which predicts $\boldsymbol{\epsilon}$ from \mathbf{x}_t . The U-Net with spatial transformer layers is applied as the architecture of the noise estimation network in common practices. For the training of DMs, a simplified variant of the variational lower bound is usually applied as the loss function to achieve high sample quality, which can be expressed as

$$\mathcal{L}_{\text{simple}} = \mathbb{E}_{t, \mathbf{x}_0, \boldsymbol{\epsilon}_t} \left[\left\| \boldsymbol{\epsilon}_t - \boldsymbol{\epsilon}_\theta(\sqrt{\bar{\alpha}_t} \mathbf{x}_0 + \sqrt{1 - \bar{\alpha}_t} \boldsymbol{\epsilon}_t, t) \right\|^2 \right]. \quad (4)$$

The binarization and quantization compress and accelerate the noise estimation model by discretizing weights and activations to low bit-width. In the baseline of the binarized diffusion model, the weight

$w \in \theta$ is binarized to 1-bit by $w^{\text{bi}} = \sigma \text{sign}(w)$ [33, 4], where sign function confine w to +1 or -1 with 0 thresholds, $w^{\text{bi}} \in \theta^{\text{bi}}$ denotes the binarized weight, and θ^{bi} denotes the binarized noise estimation network. σ is the floating-point scalar, which is initialized as $\frac{\|w\|}{n}$ (n denotes the number of weight elements) and learnable during training process following [33, 22]. The activation is quantized by the LSQ quantizer [6]. With the $32\times$ compressed weight, the computation of the noise estimation model can also be replaced with additions, achieving significant compression and acceleration.

3.2 Learnable Multi-basis Binarizer

In the current binarization process, weights are quantized to binary values to economize on storage and computation during inference. Additionally, activation can be quantized to conserve resources further. However, the extensive discretization of weights to 1-bit in DMs results in a notable deterioration of the generated representations. The limitation of each weight element’s bit-width to the original $\frac{1}{32}$ significantly diminishes the richness of filters or linear projections formed by these weights. The capability of DMs to extract features from the input is severely compromised after extreme weight discretization, which poses a challenge to the representation details of DMs in the generation process. Therefore, improving the binarization operator for DMs is critical to generating the rich detail and texture of high-quality data.

We propose a Learnable Multi-basis Binarizer (LMB) that enhances the binarization weights of DMs to achieve rich representations, selectively applied at parameter-sparse locations to minimize burden:

Binarizer Definition. In forward propagation, LMB is defined as

$$w_{\text{LMB}}^{\text{bi}} = \sigma_{\text{I}} \text{sign}(w) + \sigma_{\text{II}} \text{sign}(w - \sigma_{\text{I}} \text{sign}(w)), \quad (5)$$

where the σ_{I} and σ_{II} are learnable scalars which are initialized as $\sigma_{\text{I}}^0 = \frac{\|w\|}{n}$ and $\sigma_{\text{II}}^0 = \frac{\|w - \sigma_{\text{I}} \text{sign}(w)\|}{n}$, respectively, $\|\cdot\|$ denotes the ℓ_2 -normalization. The inference of layer binarized by LMB involves the computation of multiple bases. For instance, the convolution in binarized DM is

$$o = a \times w_{\text{LMB}}^{\text{bi}} = \sigma_{\text{I}} (a \otimes \text{sign}(w)) + \sigma_{\text{II}} (a \otimes \text{sign}(w - \sigma_{\text{I}} \text{sign}(w))), \quad (6)$$

where a denotes the activation, and \times and \otimes denote the convolution consisting of multiplication and addition instructions [33, 14], respectively. During the inference process, the computation of multiple bases involved in a certain LMB can be parallelized since they are independent, allowing the inference of binarized DM to be fully accelerated.

In the backward propagation of LMB, the gradient of the learnable scalars is calculated as follows:

$$\frac{\partial w_{\text{LMB}}^{\text{bi}}}{\partial \sigma_{\text{I}}} = \begin{cases} \text{sign}(w) (1 - \sigma_{\text{II}} \text{sign}(w)), & \text{if } \sigma_{\text{I}} \text{sign}(w) \in (w - 1, w + 1), \\ \text{sign}(w), & \text{otherwise,} \end{cases} \quad (7)$$

$$\frac{\partial w_{\text{LMB}}^{\text{bi}}}{\partial \sigma_{\text{II}}} = \text{sign}(w - \sigma_{\text{I}} \text{sign}(w)), \quad (8)$$

where the Straight Through Estimator (STE) is applied to approximate the sign function during backwards. With the binary basis with different learnable scalars, the representation capability of quantized weights can be significantly enhanced. The residual initialization makes the optimization of binarized DM start from an error-minimizing state. With LMB, the representation of weight is significantly diversified compared to the binarized DM baseline, where the statistic about the LMB is presented in Fig 3. The rich representation of LMB allows BinaryDM to have a more complete expression even beyond achieving overall denoising, as evidenced by various details in Fig 4.

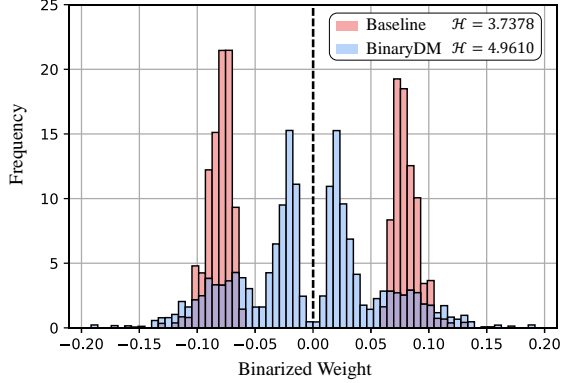


Figure 3: Comparison of filter(channel-wise) binarized weights for a convolutional layer. LMB possesses a broader representation range, while the quantitative information entropy further illustrates its enhanced representation capacity.

Location Selection. In our BinaryDM, the proposed LMB is partly applied to DMs in crucial and parameter-sparse locations while retaining concise vanilla binarization at others to avoid unnecessary additional overhead and achieve a balanced trade-off between accuracy and efficiency. Specifically, we apply LMB where the feature scale is greater or equal to $\frac{1}{2}$ input scale, *i.e.*, the first and last 6 layers with only the 15% of whole parameters in the noise estimation network of BinaryDM, while other layers keep consistent with the binarized DM baseline with vanilla binarizers. Since the smaller kernel size of weights is applied in the top and bottom locations of U-Net, our parameter-sparse location selection for LMB can significantly reduce the 41.5% cost of storage compared to applying across the whole DM directly. More importantly, the binarized units closer to the input and output of the noise estimation model are significantly improved by LMB, which is crucial for DM models: binarized units close to the input are expected to extract patterns from original data, and units close to the output directly influence the final estimation results. Therefore, the proposed LMB can significantly improve binarized DM with a minor burden.

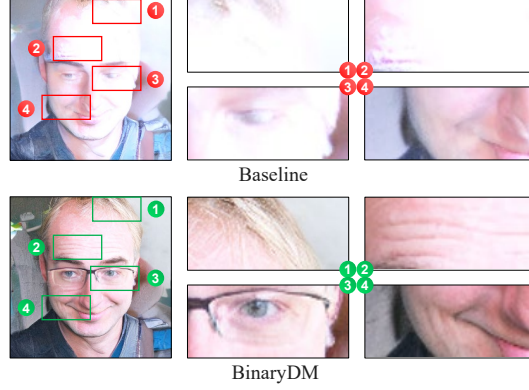


Figure 4: Comparison of details in the generated image. Compared to the baseline, BinaryDM demonstrates a richer and more intricate representation.

3.3 Low-rank Representation Mimicking

In the quantization-aware training of DMs, the discretization of parameter space caused by weight binarization and activation quantization function and the inaccurate gradient approximation involved in the derivation process bring difficulties to the stable convergence of binarized DM. Since having almost the same architecture, the original full-precision DM can be regarded as an oracle of the binarized one. Therefore, an intuitive approach is to assist the training of binarized DMs by mimicking the representation of full-precision replicas. During training, aligning outputs and/or intermediate representations of binarized DMs with full-precision counterparts can provide additional supervision, accelerating the convergence of quantized DMs significantly.

However, there are issues directly aligning the intermediate representations of binarized and full-precision DMs during optimization. Firstly, fine-grained alignment of high-dimensional representation leads to a blurry optimization direction for DMs, especially when mimicking the intermediate features is introduced. Secondly, compared to the full-precision DM, the intermediate features in the binarized one are derived from a discrete latent space since the discretization of parameters makes it difficult to mimic the full-precision DM directly.

Therefore, we propose Low-rank Representation Mimicking (LRM) to efficiently optimize the BinaryDM by mimicking full-precision representations in a low-rank space. We group the full-precision DM θ^{FP} based on the timestep embedding modules composed of residual convolution and transformer blocks. The intermediate representation can be denoted as $\hat{\epsilon}_{\theta_i}^{\text{FP}}(\mathbf{x}_t, t) \in \mathbb{R}^{h \times w \times c}$. We use principal component analysis (PCA) to project representations to low-rank space. The covariance matrix for representations of the full-precision DM is

$$C_i = \frac{1}{(h \times w)^2} \hat{\epsilon}_{\theta_i}^{\text{FP}}(\mathbf{x}_t, t) \hat{\epsilon}_{\theta_i}^{\text{FP}T}(\mathbf{x}_t, t), \quad (9)$$

where θ_i represents the composition of the top i modules. The eigenvector matrix $E_i \in \mathbb{R}^{c \times c}$ is

$$E_i^T C_i E_i = \Lambda_i, \quad (10)$$

where Λ_i is the diagonal matrix of eigenvalues of C_i , arranged in descending order. We take the matrix composed of the first $\lceil \frac{c}{K} \rceil$ column eigenvectors of E_i as the transformation matrix, denoted as $E_i^{\lceil \frac{c}{K} \rceil}$, where $\lceil \cdot \rceil$ denotes the round function and K denotes to the reduction times of dimension. We use $E_i^{\lceil \frac{c}{K} \rceil}$ to project the intermediate representation of both full-precision and binarized:

$$\mathcal{R}_i^{\text{FP}}(\mathbf{x}_t, t) = \hat{\epsilon}_{\theta_i}^{\text{FP}}(\mathbf{x}_t, t) E_i^{\lceil \frac{c}{K} \rceil}, \quad \mathcal{R}_i^{\text{bi}}(\mathbf{x}_t, t) = \hat{\epsilon}_{\theta_i}^{\text{bi}}(\mathbf{x}_t, t) E_i^{\lceil \frac{c}{K} \rceil}, \quad (11)$$

where $\hat{\epsilon}_{\theta_i}^{\text{bi}}(\mathbf{x}_t, t)$ denotes the intermediate representation of the i -th layer in the DM with binarized parameters θ^{bi} , and $\mathcal{R}_i^{\text{FP}}(\mathbf{x}_t, t)$ and $\mathcal{R}_i^{\text{bi}}(\mathbf{x}_t, t)$ denote the low-rank representations of full-precision and binarized DMs, respectively, with the same shape $h \times w \times \lceil \frac{c}{K} \rceil$. The K empirically defaults as 4 and is detailed ablated in Appendix B.3.

We then leverage the obtained low-rank representation to drive the binarized DM to learn the full-precision counterpart. We construct a mean squared error (MSE) loss between the i -th module of low-rank representations between full-precision and binarized DMs:

$$\mathcal{L}_{\text{LRM}i} = \|\mathcal{R}_i^{\text{FP}} - \mathcal{R}_i^{\text{bi}}\|. \quad (12)$$

The total loss function is composed of Eq. (4) and Eq. (12):

$$\mathcal{L}_{\text{total}} = \mathcal{L}_{\text{simple}} + \lambda \frac{1}{M} \sum_{i=1}^M \mathcal{L}_{\text{LRM}i}, \quad (13)$$

where M denotes the number of timestep embedding modules in the noise estimation network of DMs, and λ is a hyperparameter coefficient to balance the loss terms. Since the computation cost of obtaining the transformation matrix $E_i^{\lceil \frac{c}{K} \rceil}$ in LRM is significantly expensive, we compute the matrix by the first batch of input and keep it fixed during the training process. The fixed mapping between representations is also beneficial to the optimization of binarized DM from a steady perspective.

LRM enables binarized DMs to mimic the representation of full-precision counterparts, improving the optimization process by introducing additional supervision. As shown in Fig 5, LRM effectively brings the local block closer to the full-precision block. Furthermore, by applying low-rank projections based on the principal components from full-precision representations before representation mimicking, the binarized DM can be optimized along clear and stable directions, accelerating the convergence of the model. Furthermore, binarized and full-precision DMs have completely consistent architectures, making representation mimicking between them natural.

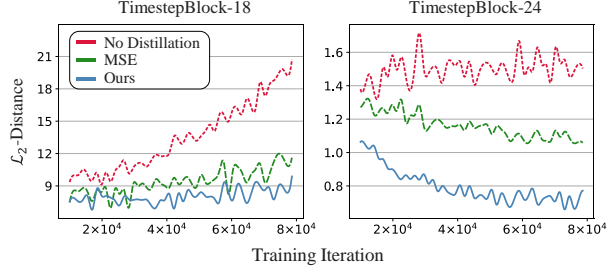


Figure 5: The impact of different distillation loss functions on the output features of each block in both full-precision DM and binary DM, measured by the \mathcal{L}_2 distance. Our proposed LRM enables the binarized DM to have the best information-mimicking capability.

3.4 Training Strategy of BinaryDM

During the training, we utilized the proposed LMB to binarize the noise estimation network of DMs and optimized it using the objective function with LRM. However, despite significant improvements in the architecture and optimization aspects, the convergence of binarized DMs remains slow and unattainable during training.

Therefore, we employed a progressive binarization strategy in the early training phase, allowing for accelerated and stable convergence of binarized DMs without incurring additional costs. As discussed in Section 1, the binarization of computational units closer to the original input and final output has a more direct and significant impact on DMs. Consequently, we quantize the $\lfloor \frac{M}{2} \rfloor$ -th timestep embedding module in the DM during the first iterations. In the subsequent $\frac{M}{2}$ -th iterations, we binarize the $(\lfloor \frac{M}{2} \rfloor - i)$ -th and $(\lfloor \frac{M}{2} \rfloor + i)$ -th modules at the i -th iteration till all modules are binarized, where $\lfloor \cdot \rfloor$ denotes the round down function. This process enables the binarized DMs to adjust to favourable starting positions for optimization. Compared to directly binarizing the entire DM at the beginning of training, this strategy demonstrates significant performance advantages

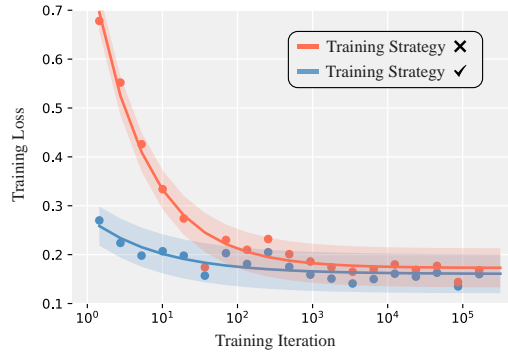


Figure 6: The impact of applying our proposed training strategy on the loss function.

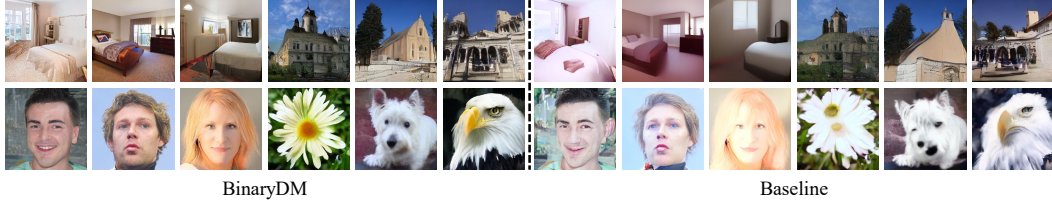


Figure 7: Visualization of samples generated by the binarized DM baseline and W1.1A4 BinaryDM.

Table 1: Comparison for unconditional generation on CIFAR-10 32×32 by DDIM with 100 steps

Method	#Bits	IS \uparrow	FID \downarrow	sFID \downarrow	Prec. \uparrow
FP	32/32	8.90	5.54	4.64	67.92
Baseline	1/32	4.21	123.78	64.31	36.88
LSQ	2/32	8.17	18.56	8.30	59.22
BinaryDM	1.1/32	8.38	10.32	5.55	62.34
Baseline	1/8	4.50	117.37	44.75	40.50
LSQ	2/8	7.64	29.66	30.63	58.76
BinaryDM	1.1/8	9.09	9.92	6.59	60.51
Baseline	1/4	1.92	318.84	115.57	2.18
LSQ	2/4	4.04	137.75	43.68	40.74
BinaryDM	1.1/4	8.11	25.83	8.46	51.22

under the same training duration, as shown in Fig 6. Additionally, it is noteworthy that the entire progressive quantization process, constituting about 0.002% (5 iterations) of the total 200K iterations usually required for training, can be considered an efficient initialization strategy for binarizing DMs.

4 Experiment

We conduct experiments on various datasets, including CIFAR-10 32×32 [17], LSUN-Bedrooms 256×256 [48], LSUN-Churches 256×256 [48], FFHQ 256×256 [16] and ImageNet 256×256 [5], for both unconditional and conditional image generation tasks over DDIM and LDM. The evaluation metrics used in our study encompass Inception Score (IS), Fréchet Inception Distance (FID) [11], Sliding Fréchet Inception Distance (sFID) [34], and Precision-and-Recall. We implement and evaluate the DMs binarized by our BinaryDM and the baseline presented in Section 3.1, where LSQ [6] is employed uniformly as activations quantizers. Several SOTA quantization methods for DMs with 2~8 bits weights are also considered [10, 18]. Detailed settings are presented in Appendix B.1.

4.1 Main Results

Unconditional Generation. We first conduct experiments on the CIFAR-10 dataset. As shown in Table 1, the binarized DM baseline suffers a severe breakdown in this low-resolution scenario, while our method significantly recovers the performance. Under the W1.1A4 bit-width, BinaryDM surpasses the binarized baseline by 6.91 in IS metrics on the CIFAR-10 and outperforms the binarized DM baseline under W1A32, where the latter involves several times of computation and storage.

Our LDM experiments encompass the evaluation of LDM-4 on LSUN-Bedrooms and FFHQ datasets, along with the assessment of LDM-8 on the LSUN-Churches dataset. The experiments utilized the DDIM sampler with 100 steps, and the detailed outcomes are presented in Table 2. The evaluation results of LDM-4 on FFHQ datasets can be found in Appendix B.2. We showcase results across various activation bit widths in the context of weight binarization, comparing them with the outcomes of some quantization methods at higher bit settings. The conventional binary baseline method exhibits subpar performance in the LDM context and experiences a further decline in the W1A4 experimental setup, particularly noticeable in the LSUN-Bedrooms dataset. In contrast, BinaryDM significantly enhances the generation quality, especially for LDM-4, exhibiting consistent performance across different activation bit settings. Notably, when compressing from W1.1A32 to W1.1A4 on the LSUN-Bedrooms dataset, the FID increased by a mere 0.69 for BinaryDM, showcasing its robustness. BinaryDM even approaches the generation quality of the full-precision model, with specifically generated image examples provided in Appendix B.4.

Table 2: Results for LDM on multiple datasets in unconditional generation by DDIM with 100 steps.

Model	Dataset	Method	#Bits	Size _(MB)	FID↓	sFID↓	Precision↑	Recall↑
LDM-4	LSUN-Bedrooms 256 × 256	FP	32/32	1045.4	3.09	7.08	65.82	45.36
		Baseline	1/32	37.3	26.43	27.65	35.43	28.00
		LSQ	2/32	69.8	7.49	12.79	64.02	37.60
		BinaryDM	1.1/32	42.1	6.42	9.63	66.92	34.98
		Baseline	1/8	37.3	21.18	25.92	39.04	29.46
		Q-Diffusion	2/8	69.8	62.01	33.56	16.48	14.12
		LSQ	2/8	69.8	6.08	11.66	62.55	38.92
		BinaryDM	1.1/8	42.1	6.60	11.63	67.23	33.48
		Baseline	1/4	37.3	39.69	35.31	26.94	22.62
		EfficientDM	4/4	134.9	10.60	-	-	-
		Q-Diffusion	4/4	134.9	427.46	277.22	0.00	0.00
		LSQ	2/4	69.8	12.95	12.79	55.97	34.30
		BinaryDM	1.1/4	42.1	7.11	11.26	62.21	33.28
		LDM-8	LSUN-Churches 256 × 256	FP	32/32	1125.2	4.82	17.66
Baseline	1/32			39.0	8.94	18.07	74.10	30.82
LSQ	2/32			74.1	8.16	19.87	74.98	35.76
BinaryDM	1.1/32			44.6	7.37	18.93	76.67	35.48
Baseline	1/8			39.0	10.43	19.52	75.10	27.64
Q-Diffusion	2/8			74.1	201.23	238.70	2.39	8.60
LSQ	2/8			74.1	8.11	19.25	77.04	34.98
BinaryDM	1.1/8			44.6	7.10	19.41	74.86	37.18
Baseline	1/4			39.0	11.94	23.06	74.81	21.96
EfficientDM	4/4			144.2	14.34	-	-	-
Q-Diffusion	4/4			144.2	198.35	184.43	5.48	0.12
LSQ	2/4			74.1	10.00	19.08	74.93	25.80
BinaryDM	1.1/4			44.6	9.71	17.79	78.63	28.60

Table 3: Results on ImageNet 256 × 256 in conditional generation by DDIM with 20 steps.

Model	Method	#Bits	IS↑	FID↓	sFID↓	Prec.↑
LDM-4	FP	32/32	235.84	12.96	25.99	92.63
	Baseline	1/32	166.06	9.13	23.16	77.32
	LSQ	2/32	184.04	9.01	22.63	84.60
	BinaryDM	1.1/32	194.80	8.50	19.14	85.99
	Baseline	1/8	167.57	10.14	25.73	78.28
	LSQ	2/8	209.29	12.04	20.32	81.79
	BinaryDM	1.1/8	210.52	9.58	20.09	87.46
	Baseline	1/4	115.92	16.92	31.31	65.73
	LSQ	2/4	187.94	11.46	22.80	76.02
	BinaryDM	1.1/4	190.36	10.40	22.09	85.73

Conditional Generation. For conditional generation, the performance of our BinaryDM is evaluated on the ImageNet dataset with a resolution of 256 × 256, focusing on LDM-4. We employ three distinct samplers to generate images: DDIM, PLMS, and DPM-Solver. The results in Table 3 underscore the remarkable effectiveness of our BinaryDM on DDIM, surpassing the baseline consistently across almost all evaluation metrics and even outperforming the full-precision diffusion model in several cases. The binarized DM baseline performs relatively stable in configurations W1A32 and W1A8 but significantly declines under W1A4, with the IS decreasing to 115. In contrast, our BinaryDM maintains an IS of 190 in W1.1A4. Moreover, our method consistently outperforms LSQ with 2-bit activation in various activation bit-widths, showcasing its outstanding performance in conditional generation tasks. The results on PLMS and DPM-Solver are shown in Appendix B.2.

4.2 Ablation Study

We perform comprehensive ablation studies for LDM-4 on the LSUN-Bedrooms 256 × 256 dataset to evaluate the effectiveness of each proposed component in BinaryDM.

We evaluate the effectiveness of our proposed LMB and LRM, and the results are presented in Table 4. The performance has shown significant recovery when applying our LMB only to binarized DM. This confirms that the degradation in parameter representational capacity due to binarization is a primary performance bottleneck in the binarized DM baseline. Solving this representation degradation is a prerequisite for improving model performance. Applying LRM in optimization alone has not fully

Table 4: Ablation results on LSUN-Bedrooms 256×256 .

Method	#Bits	FID↓	sFID↓	Prec.↑	Recall↑
FP	32/32	3.09	7.08	65.82	45.36
Vanilla	1/32	27.33	30.72	37.11	22.86
+LMB	1.1/32	10.27	13.73	64.85	32.58
+LRM	1/32	27.37	35.71	34.93	19.28
BinaryDM	1.1/32	6.42	9.63	66.92	34.98

Table 5: Inference efficiency of our proposed BinaryDM of LDM-8.

Model	Method	#Bits	Size _(MB)	OPs _($\times 10^9$)	FID↓
LDM-8	Full-Precision	4/4	1125.2	18.60	4.82
	Q-Diffusion	4/4	144.2	4.97	198.35
	EfficientDM	4/4	144.2	4.97	14.34
	LSQ	2/4	74.1	2.64	10.00
	BinaryDM	1.1/4	44.6	2.40	9.71

Table 6: Training time-cost of BinaryDM compared to the advanced PTQ method.

Dataset	Method	#Bits	Size _(MB)	Time _(h)	FID↓
LSUN-Bedrooms	Q-Diffusion	4/4	134.9	13.7	427.46
	BinaryDM	1.1/4	42.1	11.3	10.22
LSUN-Churches	Q-Diffusion	4/4	144.2	10.9	198.35
	BinaryDM	1.1/4	44.6	9.0	10.58

addressed the performance bottleneck of binarized DM, leading to a significant decrease in accuracy. Further substantiating this view, the detailed ablation experiments in Appendix B.3 delve into an in-depth discussion of the specifics concerning LMB and LRM. Combining these two techniques in BinaryDM can significantly enhance performance, emphasizing that optimization can benefit from focusing on low-ranking crucial directions when ensuring accurate representation.

We further compared our proposed progressive training strategy with the original training procedure, and the detailed specifics are also provided in Appendix B.3.

4.3 Efficiency Analysis

For inference, we demonstrate the size and OPs of BinaryDM under different activation bit-widths. The results in Table 5 indicate that our DM can achieve up to 24.8× space savings while obtaining up to 9.3× acceleration during inference, fully harnessing the advantages of binary computation.

For training, while the training process for our binarized DM typically incurs higher overhead compared to post-training quantization methods, practical observations reveal that our approach offers productivity advantages across various models and datasets. As shown in Table 6, despite having a training time shorter than the calibration time required by Q-Diffusion, our method attains significantly superior generation quality, particularly at lower bits.

Limitations. BinaryDM directly uses layerwise LSQ [6] for activations instead of specific designs, we thus believe the potential for improving BinaryDM from activation quantization perspective.

5 Conclusion

In this paper, we propose BinaryDM, a novel accurate quantization-aware training approach to push the weights of diffusion models towards the limit of binary. Firstly, we present a Learnable Multi-basis Binarizer (LMB) to recover the representations generated by the binarized DM, which design improves the detailed information in details of representations crucial to the DM. Secondly, a Low-rank Representation Mimicking (LRM) is applied to enhance the binarization-aware optimization of the DM, alleviating the optimization direction ambiguity caused by fine-grained alignment. Moreover, a progressive initialization strategy is applied to training DMs to avoid convergence difficulties. Comprehensive experiments demonstrate that BinaryDM achieves significant accuracy and efficiency gains compared to SOTA quantization methods of DMs under ultra-low bit-widths. As the first binarization method for diffusion models, W1.1A4 BinaryDM achieves impressive $9.3 \times$ OPs and $24.8 \times$ storage savings, showcasing substantial advantages and potential for deploying DMs on edge.

References

- [1] Fan Bao, Chongxuan Li, Jun Zhu, and Bo Zhang. Analytic-dpm: an analytic estimate of the optimal reverse variance in diffusion probabilistic models. *arXiv preprint arXiv:2201.06503*, 2022.
- [2] Joseph Bethge, Christian Bartz, Haojin Yang, Ying Chen, and Christoph Meinel. Meliusnet: Can binary neural networks achieve mobilenet-level accuracy? *arXiv preprint arXiv:2001.05936*, 2020.
- [3] Nanxin Chen, Yu Zhang, Heiga Zen, Ron J Weiss, Mohammad Norouzi, and William Chan. Wavegrad: Estimating gradients for waveform generation. *arXiv preprint arXiv:2009.00713*, 2020.
- [4] Matthieu Courbariaux, Itay Hubara, Daniel Soudry, Ran El-Yaniv, and Yoshua Bengio. Binarized neural networks: Training deep neural networks with weights and activations constrained to+ 1 or-1. *arXiv preprint arXiv:1602.02830*, pages 1–11, 2016.
- [5] Jia Deng, Wei Dong, Richard Socher, Li-Jia Li, Kai Li, and Li Fei-Fei. Imagenet: A large-scale hierarchical image database. In *Proceedings of the IEEE/CVF Conference on Computer Vision and Pattern Recognition*, pages 248–255. IEEE, 2009.
- [6] Steven K Esser, Jeffrey L McKinstry, Deepika Bablani, Rathinakumar Appuswamy, and Dharmendra S Modha. Learned step size quantization. In *International Conference on Learning Representations*, pages 1–12, 2019.
- [7] Gongfan Fang, Xinyin Ma, and Xinchao Wang. Structural pruning for diffusion models. *arXiv preprint arXiv:2305.10924*, 2023.
- [8] Amir Gholami, Sehoon Kim, Zhen Dong, Zhewei Yao, Michael W Mahoney, and Kurt Keutzer. A survey of quantization methods for efficient neural network inference. In *Low-Power Computer Vision*, pages 291–326. Chapman and Hall/CRC, 2022.
- [9] Ruihao Gong, Xianglong Liu, Shenghu Jiang, Tianxiang Li, Peng Hu, Jiazhen Lin, Fengwei Yu, and Junjie Yan. Differentiable soft quantization: Bridging full-precision and low-bit neural networks. In *Proceedings of the IEEE/CVF International Conference on Computer Vision*, pages 4852–4861, 2019.
- [10] Yefei He, Jing Liu, Weijia Wu, Hong Zhou, and Bohan Zhuang. Efficientdm: Efficient quantization-aware fine-tuning of low-bit diffusion models. *arXiv preprint arXiv:2310.03270*, 2023.
- [11] Martin Heusel, Hubert Ramsauer, Thomas Unterthiner, Bernhard Nessler, and Sepp Hochreiter. Gans trained by a two time-scale update rule converge to a local nash equilibrium. *Advances in neural information processing systems*, 30, 2017.
- [12] Jonathan Ho, William Chan, Chitwan Saharia, Jay Whang, Ruiqi Gao, Alexey Gritsenko, Diederik P Kingma, Ben Poole, Mohammad Norouzi, David J Fleet, et al. Imagen video: High definition video generation with diffusion models. *arXiv preprint arXiv:2210.02303*, 2022.
- [13] Jonathan Ho, Ajay Jain, and Pieter Abbeel. Denoising diffusion probabilistic models. *Advances in neural information processing systems*, 33:6840–6851, 2020.
- [14] Itay Hubara, Matthieu Courbariaux, Daniel Soudry, Ran El-Yaniv, and Yoshua Bengio. Binarized neural networks. *Advances in Neural Information Processing Systems*, 29:1–9, 2016.
- [15] Myeonghun Jeong, Hyeongju Kim, Sung Jun Cheon, Byoung Jin Choi, and Nam Soo Kim. Diff-tts: A denoising diffusion model for text-to-speech. *arXiv preprint arXiv:2104.01409*, 2021.
- [16] Tero Karras, Samuli Laine, and Timo Aila. A style-based generator architecture for generative adversarial networks. In *Proceedings of the IEEE/CVF conference on computer vision and pattern recognition*, pages 4401–4410, 2019.

- [17] Alex Krizhevsky, Geoffrey Hinton, et al. Learning multiple layers of features from tiny images. 2009.
- [18] Xiuyu Li, Yijiang Liu, Long Lian, Huanrui Yang, Zhen Dong, Daniel Kang, Shanghang Zhang, and Kurt Keutzer. Q-diffusion: Quantizing diffusion models. In *Proceedings of the IEEE/CVF International Conference on Computer Vision*, pages 17535–17545, 2023.
- [19] Yanjing Li, Sheng Xu, Xianbin Cao, Xiao Sun, and Baochang Zhang. Q-dm: An efficient low-bit quantized diffusion model. In *Thirty-seventh Conference on Neural Information Processing Systems*, 2023.
- [20] Yuhang Li, Ruihao Gong, Xu Tan, Yang Yang, Peng Hu, Qi Zhang, Fengwei Yu, Wei Wang, and Shi Gu. Brecq: Pushing the limit of post-training quantization by block reconstruction. In *International Conference on Learning Representations*, pages 1–16, 2020.
- [21] Yang Lin, Tianyu Zhang, Peiqin Sun, Zheng Li, and Shuchang Zhou. Fq-vit: Post-training quantization for fully quantized vision transformer. *arXiv preprint arXiv:2111.13824*, 2021.
- [22] Zechun Liu, Zhiqiang Shen, Marios Savvides, and Kwang-Ting Cheng. Reactnet: Towards precise binary neural network with generalized activation functions. In *Proceedings of the European Conference on Computer Vision*, pages 143–159. Springer, 2020.
- [23] Weijian Luo. A comprehensive survey on knowledge distillation of diffusion models. *arXiv preprint arXiv:2304.04262*, 2023.
- [24] Kangfu Mei and Vishal Patel. Vidm: Video implicit diffusion models. In *Proceedings of the AAAI Conference on Artificial Intelligence*, volume 37, pages 9117–9125, 2023.
- [25] Chenlin Meng, Robin Rombach, Ruiqi Gao, Diederik Kingma, Stefano Ermon, Jonathan Ho, and Tim Salimans. On distillation of guided diffusion models. In *Proceedings of the IEEE/CVF Conference on Computer Vision and Pattern Recognition*, pages 14297–14306, 2023.
- [26] Gautam Mittal, Jesse Engel, Curtis Hawthorne, and Ian Simon. Symbolic music generation with diffusion models. *arXiv preprint arXiv:2103.16091*, 2021.
- [27] Markus Nagel, Rana Ali Amjad, Mart Van Baalen, Christos Louizos, and Tijmen Blankevoort. Up or down? adaptive rounding for post-training quantization. In *International Conference on Machine Learning*, pages 7197–7206. PMLR, 2020.
- [28] Alexander Quinn Nichol and Prafulla Dhariwal. Improved denoising diffusion probabilistic models. In *International Conference on Machine Learning*, pages 8162–8171. PMLR, 2021.
- [29] Chenhao Niu, Yang Song, Jiaming Song, Shengjia Zhao, Aditya Grover, and Stefano Ermon. Permutation invariant graph generation via score-based generative modeling. In *International Conference on Artificial Intelligence and Statistics*, pages 4474–4484. PMLR, 2020.
- [30] Vadim Popov, Ivan Vovk, Vladimir Gogoryan, Tasnima Sadekova, and Mikhail Kudinov. Grad-tts: A diffusion probabilistic model for text-to-speech. In *International Conference on Machine Learning*, pages 8599–8608. PMLR, 2021.
- [31] Haotong Qin, Ruihao Gong, Xianglong Liu, Xiao Bai, Jingkuan Song, and Nicu Sebe. Binary neural networks: A survey. *Pattern Recognition*, 105:107281, 2020.
- [32] Haotong Qin, Xiangguo Zhang, Ruihao Gong, Yifu Ding, Yi Xu, and Xianglong Liu. Distribution-sensitive information retention for accurate binary neural network. *International Journal of Computer Vision*, 131(1):26–47, 2023.
- [33] Mohammad Rastegari, Vicente Ordonez, Joseph Redmon, and Ali Farhadi. Xnor-net: Imagenet classification using binary convolutional neural networks. In *Proceedings of the European Conference on Computer Vision*, pages 525–542. Springer, 2016.
- [34] Tim Salimans, Ian Goodfellow, Wojciech Zaremba, Vicki Cheung, Alec Radford, and Xi Chen. Improved techniques for training gans. *Advances in neural information processing systems*, 29, 2016.

- [35] Tim Salimans and Jonathan Ho. Progressive distillation for fast sampling of diffusion models. *arXiv preprint arXiv:2202.00512*, 2022.
- [36] Robin San-Roman, Eliya Nachmani, and Lior Wolf. Noise estimation for generative diffusion models. *arXiv preprint arXiv:2104.02600*, 2021.
- [37] Yuzhang Shang, Zhihang Yuan, Bin Xie, Bingzhe Wu, and Yan Yan. Post-training quantization on diffusion models. In *Proceedings of the IEEE/CVF Conference on Computer Vision and Pattern Recognition*, pages 1972–1981, 2023.
- [38] Jiaming Song, Chenlin Meng, and Stefano Ermon. Denoising diffusion implicit models. *arXiv preprint arXiv:2010.02502*, 2020.
- [39] Yang Song and Stefano Ermon. Generative modeling by estimating gradients of the data distribution. *Advances in neural information processing systems*, 32, 2019.
- [40] Yang Song, Jascha Sohl-Dickstein, Diederik P Kingma, Abhishek Kumar, Stefano Ermon, and Ben Poole. Score-based generative modeling through stochastic differential equations. *arXiv preprint arXiv:2011.13456*, 2020.
- [41] Ziwei Wang, Han Xiao, Jiwen Lu, and Jie Zhou. Generalizable mixed-precision quantization via attribution rank preservation. In *Proceedings of the IEEE/CVF International Conference on Computer Vision*, pages 5291–5300, 2021.
- [42] Daniel Watson, Jonathan Ho, Mohammad Norouzi, and William Chan. Learning to efficiently sample from diffusion probabilistic models. *arXiv preprint arXiv:2106.03802*, 2021.
- [43] Xiuying Wei, Ruihao Gong, Yuhang Li, Xianglong Liu, and Fengwei Yu. Qdrop: Randomly dropping quantization for extremely low-bit post-training quantization. *arXiv preprint arXiv:2203.05740*, 2022.
- [44] Yixing Xu, Kai Han, Chang Xu, Yehui Tang, Chunjing Xu, and Yunhe Wang. Learning frequency domain approximation for binary neural networks. *Advances in Neural Information Processing Systems*, 34:25553–25565, 2021.
- [45] Zihan Xu, Mingbao Lin, Jianzhuang Liu, Jie Chen, Ling Shao, Yue Gao, Yonghong Tian, and Rongrong Ji. Recu: Reviving the dead weights in binary neural networks. In *Proceedings of the IEEE/CVF International Conference on Computer Vision*, pages 5198–5208, 2021.
- [46] Jiaming Yang, Chenwei Tang, Caiyang Yu, and Jiancheng Lv. Gwq: Group-wise quantization framework for neural networks. In *Asian Conference on Machine Learning*, pages 1526–1541. PMLR, 2024.
- [47] Jiwei Yang, Xu Shen, Jun Xing, Xinmei Tian, Houqiang Li, Bing Deng, Jianqiang Huang, and Xian-sheng Hua. Quantization networks. In *Proceedings of the IEEE/CVF Conference on Computer Vision and Pattern Recognition*, pages 7308–7316, 2019.
- [48] Fisher Yu, Ari Seff, Yinda Zhang, Shuran Song, Thomas Funkhouser, and Jianxiong Xiao. Lsun: Construction of a large-scale image dataset using deep learning with humans in the loop. *arXiv preprint arXiv:1506.03365*, 2015.

A Details of BinaryDM

Diffusion Models have showcased remarkable performance across a diverse array of tasks [13, 39, 40, 29, 26, 30, 15]. These tasks involve a forward Markov chain process, wherein generated noisy samples are incrementally added through Gaussian noise. Subsequently, a reverse denoising process refines these samples, producing high-fidelity images. However, the diffusion model’s slow generation process poses a significant challenge to widespread implementation. To address this issue, substantial research has concentrated on reducing the number of time steps required for diffusion model generation. Techniques such as trajectory search can be formulated as dynamic programming problems [42], and grid search has demonstrated the ability to discover effective trajectories within a mere six-time steps [3]. Moreover, the introduction of non-Markov diffusion processes has been instrumental in expediting sampling during the reverse process [39, 40], with the application of numerical methods to solve associated equations resulting in a notable reduction in the number of iterations to just a few dozen. Efforts to address these challenges have led to the exploration of faster step size schedules for VP diffusions, demonstrating the ability to maintain relatively good quality and diversity metrics [36]. Additionally, analytical approximations have been derived to simplify the generation process [1]. These developments mark strides towards enhancing the efficiency and practicality of diffusion models in various applications. Despite these advancements, the denoising models still involve a considerable number of parameters, demanding substantial computation and memory resources for each denoising step. This computational expense hinders the practical implementation of the inference process on standard hardware.

Quantization and Binarization are popular compression approaches [27, 20, 43, 21], which quantize the full-precision parameters of the neural network to lower bit-width (*e.g.*, 1-8 bit). By converting floating-point weight and activation into quantized ones, the model size of the neural network can be decreased, and the computational complexity can also be reduced, leading to significant inference speedup, memory usage saving, and lower energy consumption. Model quantization methods for diffusion models are generally divided into two categories based on their pipeline and resource access during training or fine-tuning: post-training quantization [37, 18] and quantization-aware training [19, 10]. As a training-free method, post-training quantization is considered a more practical solution to obtain quantized models at low cost by searching for the best scaling factor candidates and optimizing the calibration strategy. However, the diffusion models quantized by post-training methods dramatically degrade generation quality [37, 18]. Thus, quantization-aware training emerges for pushing quantized neural networks to higher accuracy [19, 10]. Benefiting from the training/fine-tuning process with sufficient data and training resources, the low-bit diffusion model obtained by quantization-aware training methods usually achieves higher accuracy than post-training ones. However, binarization for the weight of diffusion models is still far from available since it suffers serious accuracy degeneration challenges in existing methods.

B Experiments and Visualization

B.1 Experiment Settings

Experimental Hardware. All our experiments were conducted on a server with Intel Xeon 462 Gold 2.40@GHz CPU and NVIDIA A800 80GB GPU.

Models and Dataset. We perform comprehensive experiments encompassing unconditional image generation and conditional image generation tasks on two diffusion models: pixel-space diffusion model DDIM and latent-space diffusion model LDM. Specifically, we conduct experiments on DDIM using the CIFAR-10 dataset with a resolution of 32×32 . For LDM, our investigations spanned multiple datasets, including LSUN-Bedrooms, LSUN-Churches, and FFHQ, all with a resolution of 256×256 . Furthermore, we employ LDM for conditional image generation on the ImageNet dataset with a resolution of 256×256 . This diverse set of experiments, conducted on different models, datasets, and tasks, allows us to validate the effectiveness of our proposed method comprehensively.

Proposed Quantization Baselines. We use per-channel quantizers for weights and per-layer quantizers, as is a common practice. To the best of our knowledge, the weights of the diffusion model have not yet been binarized, and we found in our initial attempts that the basic BNN without scaling factors would collapse directly at the beginning of training. Hence, we utilize the fundamental binary quantizer, as outlined in Section 3.1, as the baseline for weight quantization, and LSQ serves as

the foundational method for activations quantization. Under the uniform premise that the weights are binarized, we use a variety of quantization bit-widths for activations to cover as many realistic situations as possible. It’s crucial to emphasize that we only quantize the diffusion model without quantizing the VAE part of the LDM. Additionally, we maintain full precision for the first and last layers, adhering to a common practice in this context.

Pipeline and hyperparameters. Our quantization-aware training (QAT) is based on the pre-trained diffusion model, and the quantizer parameters and latent weights are trained simultaneously. The overall training process is relatively consistent with the original training process of DDIM or LDM. Relative to the training hyperparameters of the full precision model, we adjust the learning rate, reducing it to one-tenth to one-hundredth of the corresponding rate in the original full precision training script, especially on certain datasets, such as CIFAR-10 and ImageNet. For DDIM training, we set the batch size to 64, while for LDM training, the batch size is configured as 4. Typically, models are trained for around 200K iterations.

Training Strategy. In addition to the baseline, the default adoption of the progressive binarization strategy, as detailed in Section 3.4, is implemented without explicit elaboration. We consider each set of 3 TimestepEmbedSequential as a granularity for progressive training and initiate separate training by selecting the middle block as the first block. For LDM-4, featuring input and output blocks with 12 modules, full binary training commences after an initial five iterations.

Evaluation. To assess the generation quality of the diffusion model, we utilize several evaluation metrics, including Inception Score (IS), Fréchet Inception Distance (FID), Sliding Fréchet Inception Distance (sFID), and Precision-and-Recall. In each evaluation, we randomly generate 50,000 samples from the model and compute the metrics using reference batches. The reference batches used to evaluate FID and sFID contain all the corresponding datasets, while only 10,000 images were extracted when Precision and Recall were calculated. We recorded FID, sFID, and Precision for all tasks and additional IS for CIFAR-10 and ImageNet. These metrics are all evaluated using ADM’s TensorFlow evaluation suite.

Efficiency. We utilize Time and OPs as metrics for evaluating training efficiency and theoretical inference efficiency, respectively. For OPs, taking the convolutional unit as an example, the BOPs definition for binary convolution operations is as follows [46, 41]:

$$BOPs \approx whmnk^2b_a b_w. \tag{14}$$

It is composed of b_w bits for weights, b_a bits for activation, n input channels, m output channels, a $k \times k$ convolutional kernel, and output dimensions of width w and height h for each channel. As there might also be full-precision modules in the model, the total OPs of the model are summed up according to the following method [2]:

$$OPs = \left(\frac{1}{64}BOPs + FLOPs\right). \tag{15}$$

B.2 Quantitative Results

The evaluation results of LDM-4 on FFHQ datasets are shown in Table 7. It can be observed that BinaryDM outperforms all other methods under various settings in terms of sFID, even surpassing W8A8 Q-Diffusion with a bit-width of W1.1A8. Moreover, BinaryDM demonstrates more significant advantages at lower activation bit-widths, achieving accurate generation with an FID of 12.99 under 4-bit activation, outperforming 2-bit LSQ.

The results on PLMS and DPM-Solver are shown in Table 8. Specifically, when utilizing the DPM-Solver sampler, the IS plummets to 85.99, and the FID experiences a sharp increase to 25.85. In stark contrast, our binarized DM maintains consistently high performance, achieving a 156.19 IS and an 11.15 FID and outperforming the baseline in most scenarios.

B.3 Additional Results

Effects of LMB. The results in Table 9 demonstrate that fully implementing the LMB yields improved outcomes, notably reducing the FID to as low as 4.35. However, this enhanced performance comes at the cost of significantly increased computational overhead. On the other hand, our plug-and-play LMB module provides binarized diffusion models with the flexibility to make a trade-off between achieving enhanced production performance and managing resource consumption.

Table 7: Results for LDM on FFHQ 256×256 in unconditional generation.

Model	Dataset	Method	#Bits	Size _(MB)	FID↓	sFID↓	Precision↑	Recall↑
LDM-4	FFHQ 256 × 256	FP	32/32	1045.4	6.64	14.16	76.88	50.82
		Q-Diffusion	4/32	134.9	11.60	10.30	-	-
		LSQ	2/32	69.8	8.46	8.76	72.68	44.33
		Baseline	1/32	37.3	13.88	12.39	74.67	34.14
		BinaryDM	1.1/32	42.1	8.31	8.18	71.59	44.49
		Q-Diffusion	8/8	265.0	10.87	10.01	-	-
		Q-Diffusion	4/8	134.9	11.45	9.06	-	-
		LSQ	2/8	69.8	7.66	8.82	73.92	42.10
		Baseline	1/8	37.3	24.17	22.34	66.73	34.52
		BinaryDM	1.1/8	42.1	8.15	8.14	74.29	42.65
		LSQ	2/4	69.8	16.50	12.16	67.71	37.72
		Baseline	1/4	37.3	24.36	22.94	67.67	25.89
		BinaryDM	1.1/4	42.1	12.99	11.55	70.04	39.55

Table 8: More results for LDM-4 on ImageNet 256 × 256 in conditional generation by different samplers.

Sampler	Method	#Bits	IS↑	FID↓	sFID↓	Prec.↑	
PLMS	FP	32/32	247.38	13.54	18.85	94.22	
	LSQ	2/32	207.56	8.74	23.41	85.34	
	Baseline	1/32	177.35	8.53	21.21	80.33	
	BinaryDM	1.1/32	203.67	8.48	19.81	86.52	
	LSQ	2/8	213.71	9.05	20.40	85.14	
	Baseline	1/8	184.89	8.92	24.52	82.98	
	BinaryDM	1.1/8	216.04	9.93	19.73	88.10	
	LSQ	2/4	165.59	11.45	25.93	73.29	
	Baseline	1/4	119.03	17.64	31.40	65.42	
	BinaryDM	1.1/4	174.17	9.44	23.36	83.65	
	DPM-Solver	FP	32/32	242.27	13.10	19.82	93.53
		LSQ	2/32	194.73	10.02	24.40	81.54
		Baseline	1/32	150.78	11.43	23.71	72.34
		BinaryDM	1.1/32	209.34	9.78	23.57	89.00
LSQ		2/8	202.58	13.11	22.69	81.81	
Baseline		1/8	167.14	9.55	26.55	77.94	
BinaryDM		1.1/8	201.50	10.41	22.11	84.82	
LSQ		2/4	156.08	17.39	29.52	62.36	
Baseline		1/4	85.99	25.85	37.39	54.94	
BinaryDM		1.1/4	156.19	11.15	26.34	79.45	

Table 9: The impact of different LMB application scopes on LSUN-Bedrooms.

Scope	#Bits	Size _(MB)	FID↓	sFID↓	Prec.↑	Recall↑
None	1/32	37.3	27.33	30.72	37.11	22.86
Half	1.1/32	42.1	6.42	9.63	66.92	34.98
Whole	2.0/32	69.7	4.35	8.51	66.93	39.94

Besides applying LMB to the usual setting of the first and last six Timestep Embed Blocks of DM, we can also apply LMB to different ranges, enabling our binarized model to achieve a more flexible balance between accuracy and efficiency. Table 10 shows the model size and computational overhead when LMB is applied to different ranges, where BinaryDM-*i* represents LMB being applied to the first and last *i* Timestep Embed Blocks of the DM. As illustrated in Table 10 and Figure 1, when LMB is applied to the first and last six Timestep Embed Blocks (i.e., BinaryDM-6 in the table), our BinaryDM achieves excellent computational overhead and high accuracy, thereby striking a balance between accuracy and efficiency.

Table 10: The results under 4-bit activation quantization on LSUN-Bedrooms.

Method	#Bits	Size(MB)	BOPs($\times 10^9$)	FLOPs($\times 10^9$)	OPs($\times 10^9$)	FID \downarrow
Q-Diffusion	4/4	134.9	1535.5	0.32	24.3	427.46
EfficientDM	4/4	134.9	1535.5	0.32	24.3	10.60
Q-DM	2/4	69.8	767.7	0.32	12.3	11.72
Q-DM	1/4	37.3	383.9	0.32	6.3	30.85
TDQ	2/4	69.8	767.7	0.32	12.3	12.36
TDQ	1/4	37.3	383.9	0.32	6.3	30.68
LSQ	2/4	69.8	767.7	0.32	12.3	12.95
Baseline	1/4	37.3	383.9	0.32	6.3	39.69
BinaryDM-0	1/4	37.3	383.9	0.32	6.3	20.38
BinaryDM-1	1.01/4	37.5	407.7	0.33	6.7	16.56
BinaryDM-2	1.02/4	37.8	446.4	0.33	7.3	12.34
BinaryDM-3	1.03/4	38.2	493.2	0.33	8.0	11.21
BinaryDM-4	1.06/4	39.2	547.7	0.34	8.9	8.62
BinaryDM-5	1.10/4	40.6	589.6	0.35	9.6	8.49
BinaryDM-6	1.14/4	42.1	638.9	0.36	10.3	7.11
BinaryDM-7	1.22/4	44.5	671.2	0.38	10.9	6.24
BinaryDM-8	1.31/4	47.6	695.5	0.41	11.3	6.62
BinaryDM-9	1.41/4	50.9	722.5	0.44	11.7	5.85
BinaryDM-10	1.55/4	55.3	737.2	0.47	12.0	5.79
BinaryDM-11	1.72/4	60.6	748.2	0.52	12.2	5.89
BinaryDM-12	1.89/4	66.1	759.5	0.56	12.4	5.43
BinaryDM-13	2.01/4	70.2	767.7	0.60	12.6	5.35

Due to the small yet important parameters at both ends of the DM, our BinaryDM prioritizes applying LMB to the heads and tails of the DM, significantly improving performance with minimal additional parameter cost. For comparison, Table 11 presents the results of applying LMB to the middle part of the DM, where *Head and Tail Parts* refers to applying LMB to the first and last 6 Timestep Embed Blocks of the DM and *Central Parts* refers to applying LMB to the middle 13 Timestep Embed Blocks. It can be observed that applying LMB only in the middle parts, despite its efficiency, does not match the performance or results achieved by the original BinaryDM approach, which solely applies LMB in the head and tail parts. Furthermore, it’s worth noting that applying LMB to the entire model does yield good results. However, since LMB already covers the head and tail parts, the original BinaryDM approach strikes the best balance between performance and efficiency.

Table 11: The results of applying LMB to different parts.

Head and Tail Parts	Central Parts	Size(MB)	FID \downarrow	sFID \downarrow	Precision \uparrow	Recall \uparrow
-	-	37.3	27.33	30.72	37.11	22.86
-	✓	65.1	11.01	17.67	51.23	40.00
✓	-	42.1	6.42	9.63	66.92	34.98
✓	✓	70.2	4.35	8.51	66.93	39.94

Considering the extensibility of LMB, we apply it to high-precision quantization. Table 12 includes results for 3-basis and 4-basis on LSUN-Bedrooms. It’s important to note that the improvement in generation performance brought about by more-basis operators exhibits diminishing returns. Alongside the relatively limited benefits, there is an increase in inference burden and more incredible difficulty in training optimization. Therefore, a partial 2-basis approach is a more effective design.

Effects of LRM. We evaluate the performance of our binarized diffusion model under various values of K (reduction times of dimension) when incorporating LRM. Additionally, we compare these results with the outcomes of applying MSE distillation directly to the output features of blocks without dimensionality reduction. The experiments reveal the model’s generation capability improves effectively when an appropriate degree of dimension reduction is employed, as illustrated in Table 13.

Table 12: The results of applying LMB to high-precision quantization.

Basis of the LMB	Model Size(MB)	FID↓	sFID↓	Precision↑
1	37.3	27.33	30.72	37.11
2	42.1	6.42	9.63	66.92
3	46.9	5.90	10.41	62.24
4	51.7	5.29	9.96	64.94

Table 13: In the application of LRM, the impact of different reduction times of dimension on the experimental results on LSUN-Bedrooms.

$\mathcal{L}_{\text{distil}}$	K	#Bits	FID↓	sFID↓	Prec.↑	Recall↑
\mathcal{L}_{MSE}	-	1.1/32	6.81	10.04	67.68	35.02
	2	1.1/32	6.67	9.36	66.53	35.66
\mathcal{L}_{LRM}	4	1.1/32	6.42	9.63	66.92	34.98
	8	1.1/32	5.85	9.55	69.35	35.32

Effects of Training Strategy. While our progressive binarization strategy at the early training phase directly influences only a limited number of iterations, its impact on the final results is remarkably significant. The results, as shown in Table 14, indicate a notable decrease in FID from 9.61 to 6.42 when the policy is applied to the binarized DM.

Table 14: The impact of the training strategy on LSUN-Bedrooms.

Strategy	#Bits	FID↓	sFID↓	Prec.↑	Recall↑
Vanilla	1.1/32	9.61	13.01	58.01	30.50
BinaryDM	1.1/32	6.42	9.63	66.92	34.98

Analysis of applying LRM to other quantization precisions. We tested the results on LSUN-Bedrooms under the following three conditions at 2/4-bit: (1) w/o distil (2) w/ distillation baseline(mse) (3) w/ LRM. The results are shown in Table 15. It can be seen that LRM consistently improves low-bit quantization models. However, it is worth noting that the performance improvement of LRM is most significant on BinaryDM, while it is less effective at 4-bit compared to the naive MSE approach. This is because LRM is still a method designed towards binary DMs. It aims to better align binary and full-precision abstract representations by reducing to a low-rank space, thereby avoiding the optimization direction ambiguity caused by direct high-dimensional fine-grained alignment.

Table 15: The results of applying LRM to other quantization precisions.

Structure	#Bits	$\mathcal{L}_{\text{distill}}$	FID↓	sFID↓	Precision↑
LMB	1.1/32	-	10.27	13.73	64.85
LMB	1.1/32	\mathcal{L}_{MSE}	6.81	10.04	67.68
LMB	1.1/32	\mathcal{L}_{LRM}	6.42	9.63	66.92
LSQ	2/32	-	7.49	12.79	64.02
LSQ	2/32	\mathcal{L}_{MSE}	7.11	13.14	61.72
LSQ	2/32	\mathcal{L}_{LRM}	7.00	12.45	62.91
LSQ	4/32	-	8.04	15.64	55.27
LSQ	4/32	\mathcal{L}_{MSE}	5.30	11.97	62.70
LSQ	4/32	\mathcal{L}_{LRM}	5.79	10.75	63.49

Applying 2-bit quantizer to achieve mix-precision. We supplement the mix-precision and full-model 2-bit baseline results from the perspective of the structure of quantization operators. Additionally, we considered the influence of factors such as LRM to compare the performance potential of different structures more fairly. Specifically, we supplemented the following content on LSUN-Bedrooms: (1) 2-bit head and trail, w/o LRM and training strategy. (2) 2-bit head and trail, w/ LRM

and training strategy. (3) 2-bit full DM, w/ LRM and training strategy. The results are shown in Table 16. It can be seen that BinaryDM consistently outperforms models constructed with 1-bit or 2-bit baseline operators, regardless of whether these models apply LRM or use mix-precision.

Table 16: The results of using 2-bit quantizer to achieve mix-precision.

2-bit Structure	Head and Tail Parts	Central Parts	LRM	FID↓	sFID↓	Precision↑
LMB (BinaryDM)	✓	-	✓	6.42	9.63	66.92
LSQ	✓	-	-	7.45	13.21	64.16
LSQ	✓	-	✓	6.82	12.56	63.68
LSQ	✓	✓	-	7.49	12.79	64.02
LSQ	✓	✓	✓	7.00	12.45	62.91

Analysis of the results of BinaryDM compared to EfficientDM. In our experiments, we found that W1.1A4 BinaryDM outperformed W4A4 efdm, which also utilizes the QAT method. Therefore, we conducted a further analysis of it. First, it can be observed that the 1-bit Baseline outperforms the 4-bit EfficientDM from Table 2. This is mainly due to the whole-model finetuning. Specifically, we trained all latent weights and quantizer parameters of the model. At the same time, EfficientDM is an efficient implementation using LoRA, and its lighter training structure, while improving efficiency, also incurs some performance sacrifices, as shown in Table 4. Additionally, the original dataset is always visible in our training process, whereas EfficientDM is a data-free quantization method. Furthermore, we investigated the effects of LRM, which requires maintaining the same training methods in the comparative experiments, allowing only structural differences. Therefore, we integrated the structure of EfficientDM into our LMB and used QALoRA to train 1/2-bit weights, with the results on LSUN-Bedrooms shown in Table 17. EfficientDM fails at extremely low bits, demonstrating why our method ultimately outperforms EfficientDM. This is due to different training strategies and inconsistent training structures.

Table 17: Effects of LRM in EfficientDM.

Method/Structure	#Bits	FID↓	sFID↓	Precision↑
Binarydm	1/4	7.11	11.26	62.21
EfficientDM	4/4	10.60	-	-
BinaryDM with QALoRA in EfficientDM	1/4	58.32	24.59	18.05

In addition, we measured the time overhead using the official code of EfficientDM. And we illustrated the changes in BinaryDM’s performance as the training duration increased. These results are presented in the Table 18, revealing that BinaryDM exhibits commendable time efficiency compared to EfficientDM and attains notable performance advantages even at extremely low bit widths. This phenomenon stems from BinaryDM’s enhanced learning capability, enabling it to effectively complete the binarization calibration process even with fewer training steps.

Table 18: Comparison of Efficiency between BinaryDM and EfficientDM on ImageNet.

Method	#Bits	Training Steps	Time(h)	IS↑	FID↓	sFID↓	Precision↑
EfficientDM	2/4	16K	2.8	3.57	189.17	106.78	11.53
BinaryDM	1.1/4	10K	1.5	51.90	36.12	27.78	48.36
BinaryDM	1.1/4	20K	3.0	94.42	19.93	28.20	63.87
BinaryDM	1.1/4	50K	7.4	129.37	12.00	25.84	74.36
BinaryDM	1.1/4	150K	22.2	163.14	10.00	22.32	80.42

B.4 Visualization Results

Visualization of the impact of LRM. As a complement to Fig 5, we present here the distance in output features between binary DM and full-precision DM on more blocks under different distillation

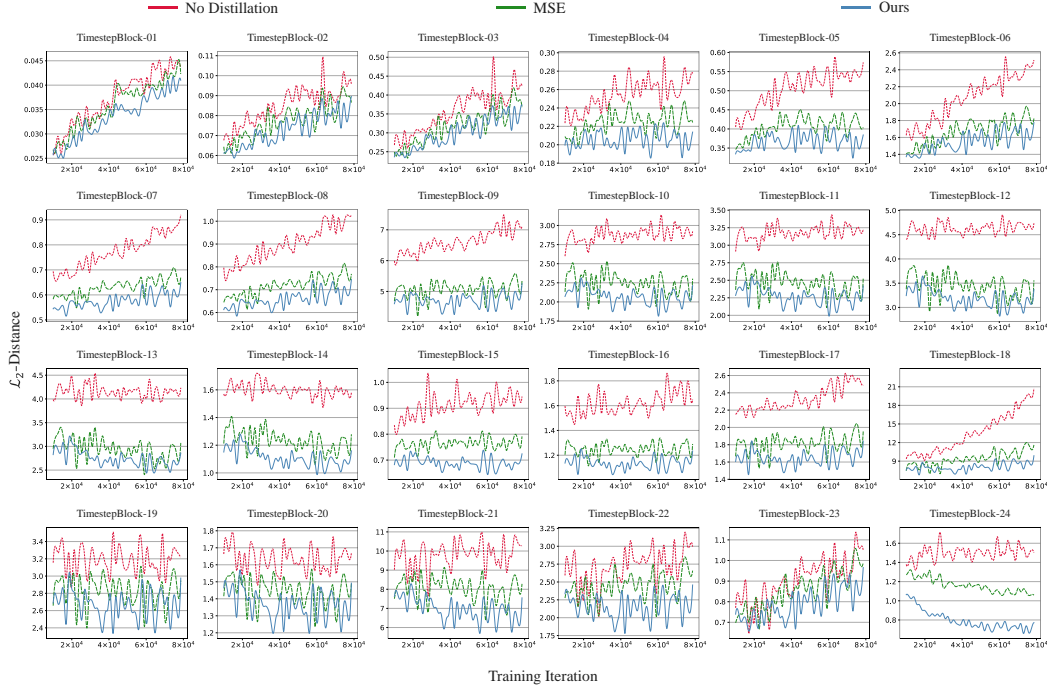
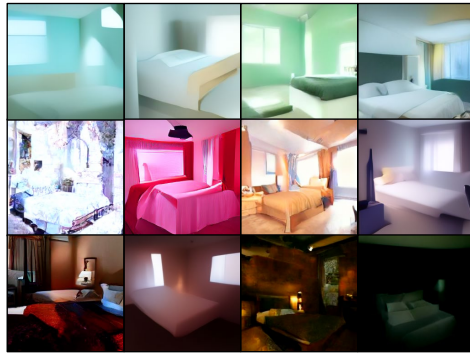


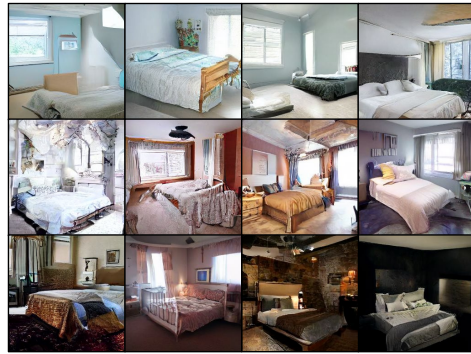
Figure 8: A comprehensive record of the impact of different distillation loss functions on the output features of each block in both full-precision DM and binarized DM, measured using the \mathcal{L}_2 distance.

losses. As shown in Fig 8, our proposed PCA-based distillation strategy consistently possesses the optimal guiding constraint capability.

Additional Random Samples. We showcase random generation results on various datasets, with unconditional generation on LSUN-Bedrooms, LSUN-Churches, and FFHQ datasets, and conditional generation on ImageNet. Overall, BinaryDM exhibits the best generation performance across datasets and maintains relatively stable performance as the activation bit-width decreases from 32 bits to 4 bits. In contrast, the Baseline not only tends to exhibit noticeable exposure errors and lacks detailed textures but also experiences significant performance degradation as the activation bit-width decreases.



Baseline (W1A4)

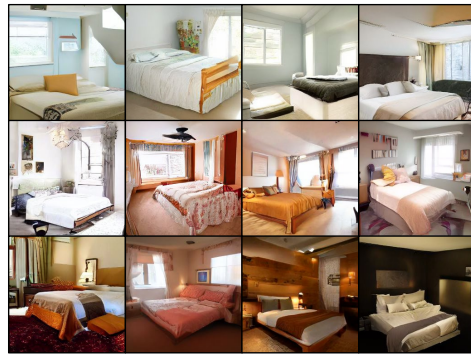


BinaryDM (W1.1A4)

Figure 9: Samples generated by 4-bit activation models on LSUN-Bedrooms 256×256

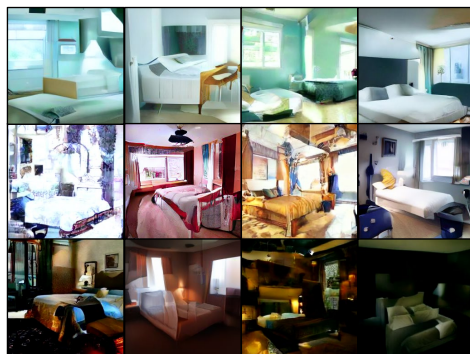


Baseline (W1A8)

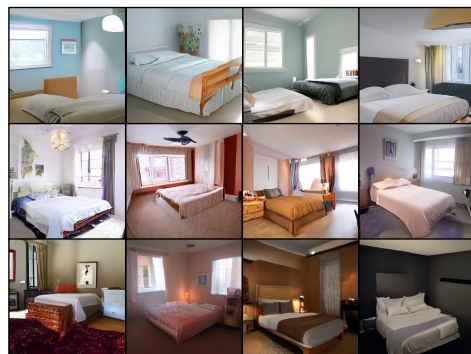


BinaryDM (W1.1A8)

Figure 10: Samples generated by 4-bit activation models on LSUN-Bedrooms 256×256



Baseline (W1A32)



BinaryDM (W1.1A32)

Figure 11: Samples generated by 4-bit activation models on LSUN-Bedrooms 256×256



Baseline (W1A4)

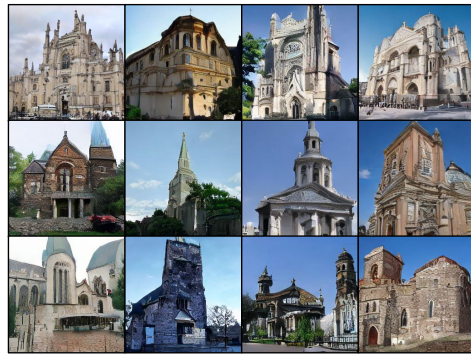


BinaryDM (W1.1A4)

Figure 12: Samples generated by 4-bit activation models on LSUN-Churches 256×256



Baseline (W1A8)

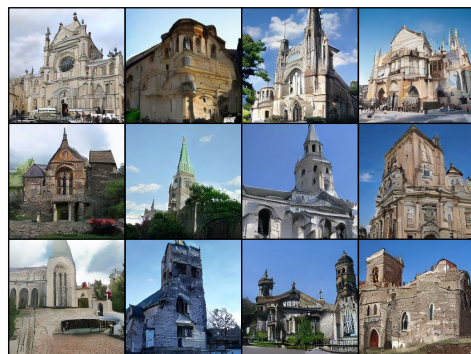


BinaryDM (W1.1A8)

Figure 13: Samples generated by 4-bit activation models on LSUN-Churches 256×256



Baseline (W1A32)



BinaryDM (W1.1A32)

Figure 14: Samples generated by 4-bit activation models on LSUN-Churches 256×256



Baseline (W1A4) BinaryDM (W1.1A4)

Figure 15: Samples generated by 4-bit activation models on FFHQ 256×256



Baseline (W1A8) BinaryDM (W1.1A8)

Figure 16: Samples generated by 4-bit activation models on FFHQ 256×256



Baseline (W1A32) BinaryDM (W1.1A32)

Figure 17: Samples generated by 4-bit activation models on FFHQ 256×256

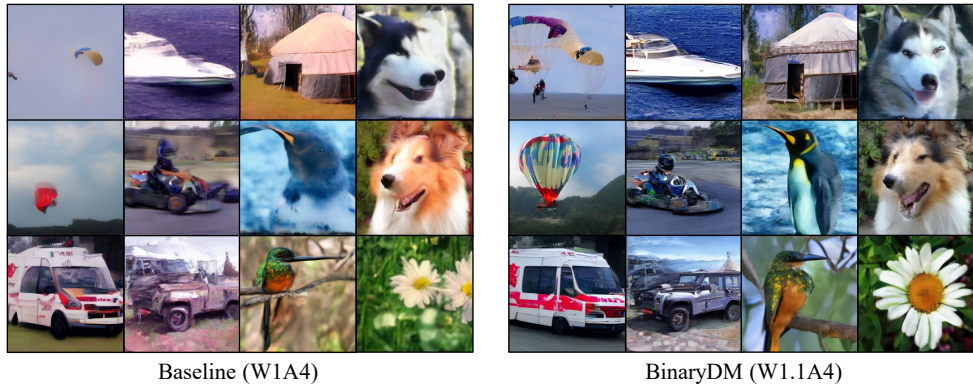


Figure 18: Samples generated by 4-bit activation models on ImageNet 256×256

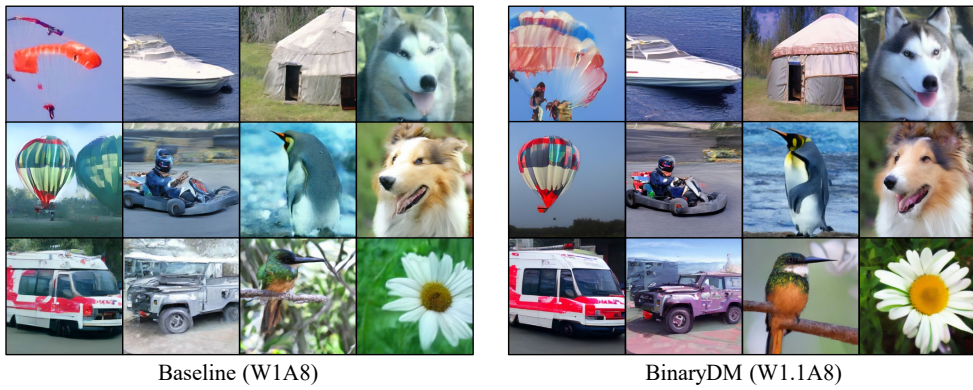


Figure 19: Samples generated by 4-bit activation models on ImageNet 256×256

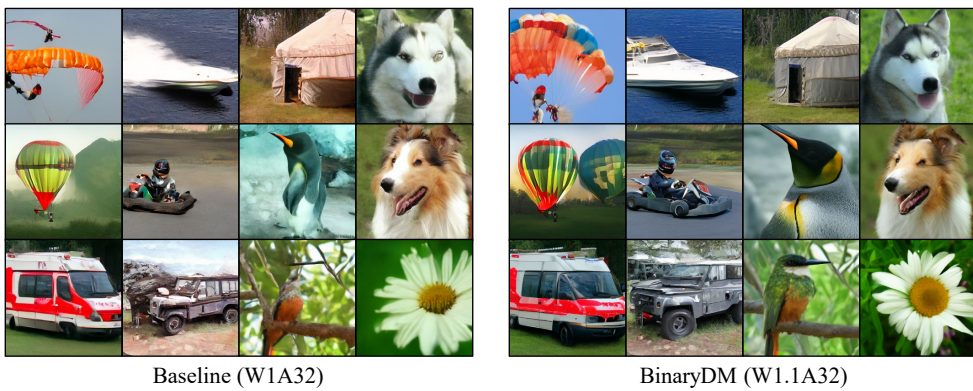


Figure 20: Samples generated by 4-bit activation models on ImageNet 256×256